Long-circulating poly(ethylene glycol)-grafted gelatin nanoparticles customized for intracellular delivery of noscapine: preparation, in-vitro characterization, structure elucidation, pharmacokinetics, and cytotoxicity analyses

Jitender Madan[c], Neerupma Dhiman[a], Satish Sardana[c], Ritu Aneja[d], Ramesh Chandra[a,b] and Anju Katyal[a]

Noscapine, the tubulin-binding anticancer agent, when administered orally, requires high ED_{50} (300–600 mg/kg), whereas intravenous administration (10 mg/kg) results in rapid elimination of the drug with a half-life of 0.39 h. Hence, the development of long-circulating injectable nanoparticles can be an interesting option for designing a viable formulation of noscapine for anticancer activity. Noscapine-enveloped gelatin nanoparticles and poly(ethylene glycol)-grafted gelatin nanoparticles were constructed and characterized. Data indicate that smooth and spherical shaped nanoparticles of 127 ± 15 nm were engineered with maximum entrapment efficiency of 65.32 ± 3.81%. Circular dichroism confirms that nanocoacervates retained the α-helical content of gelatin in ethanol whereas acetone favored the formation of a random coil. Moreover, the Fourier transform infrared and powder X-ray diffraction pattern prevents any significant change in the noscapine-loaded gelatin nanoparticles in comparison with individual components. In-vitro release kinetic data suggest a first-order release of noscapine (85.1%) from gelatin nanoparticles with a release rate constant of 7.611×10^{-3}. It is to be noted that there is a 1.43-fold increase in the area under the curve up to the last sampling point for the noscapine-loaded poly(ethylene glycol)-grafted gelatin nanoparticles over the noscapine-loaded gelatin nanoparticles and a 13.09-fold increase over noscapine. Cytotoxicity analysis of the MCF-7 cell line indicated that the IC_{50} value of the noscapine-loaded poly(ethylene glycol)-grafted gelatin nanoparticles was equivalent to 20.8 μmol/l, which was significantly ($P < 0.05$) lower than the IC_{50} value of the noscapine-loaded gelatin nanoparticles (26.3 μmol/l) and noscapine (40.5 μmol/l). Noscapine-loaded poly(ethylene glycol)-grafted gelatin nanoparticles can be developed as a promising therapeutic agent for the management of breast cancer. *Anti-Cancer Drugs* 22:543–555 © 2011 Wolters Kluwer Health | Lippincott Williams & Wilkins.

Anti-Cancer Drugs 2011, **22**:543–555

Keywords: cytotoxicity, gelatin nanoparticles, noscapine, pharmacokinetic

[a]Dr B.R. Ambedkar Centre for Biomedical Research, [b]Department of Chemistry, University of Delhi, Delhi, [c]Department of Pharmaceutics, Hindu College of Pharmacy, Sonepat, Haryana, India and [d]Department of Biology, Georgia State University, Atlanta, Georgia, USA

Correspondence to Anju Katyal, PhD, Dr B.R Ambedkar Centre for Biomedical Research, University of Delhi, Delhi 110007, India
Tel: +91 11 27666272; fax: +91 11 27666248;
e-mail: anju_katyal@yahoo.com

Received 15 April 2010 **Revised form accepted** 8 October 2010

Introduction

Noscapine (NOS) is a novel tubulin-binding, antiangiogenic anticancer drug that causes cell cycle arrest and induces apoptosis in cancer cells both *in vitro* and *in vivo* [1–4]. It is a weak base (pK_a of approximately 7.8) with 44.69% absolute bioavailability and an oral half-life of 1.33 h, necessitating its frequent administration in large doses (ED_{50} of approximately 300–600 mg/kg bodyweight) to act as an anticancer agent [5–8]. Moreover, its low aqueous solubility and extensive first-pass metabolism further hamper the development of orally controlled release of an anticancer formulation of NOS [9]. Recently, a soluble molecular inclusion complex of NOS with β-cyclodextrin has been synthesized in our laboratory to augment aqueous solubility and oral bioavailability [6]. In contrast, the short biological half-life (0.39 h) after intravenous administration (10 mg/kg) causes rapid elimination of the drug from the body by first-order kinetics, leading to low drug disposition in the tumor mass [7]. Coupled with these limitations, the intratumor microenvironment is intrinsically acidic owing to the deposition of lactic acid as a result of increased aerobic and anaerobic glycolysis by the tumor cells. In general, the extracellular pH in the tumor mass is below 7.0, whereas the intracellular pH is maintained at a neutral range by buffer mechanisms. The low pH gradient markedly affects the response of tumors to various anticancer drugs. The acidic pH augments the cellular uptake of weakly acidic drugs such as cyclophosphamide and cisplatin owing to the un-ionization effect, whereas it retards the uptake of weakly basic drugs such as doxorubicin and vinblastine owing to ionization [10]. Hence, to overcome these limitations, the development of injectable nanoparticles with a prolonged half-life is the most suitable option, which can serve as a customized, drug delivery cargo that is capable of ferrying chemotherapeutic agents into

0959-4973 © 2011 Wolters Kluwer Health | Lippincott Williams & Wilkins DOI: 10.1097/CAD.0b013e32834159b8

Copyright © Lippincott Williams & Wilkins. Unauthorized reproduction of this article is prohibited.

malignant cells while at the same time sparing healthy cells. These novel, dispersed particulate carriers of less than 1 μm diameter, particularly ranging between a few nanometers to 500 nm in size, hold promise to overcome biological, biophysical, and biomedical barriers [11]. It is apparent that the polymers, the building blocks of nanoparticulate composites, belong to natural or synthetic origins and in this regard, various polymers have been exploited for their biomedical applications [12]. Gelatin is a natural polymer commonly used as a drug carrier matrix. Biodegradability, nonimmunogenicity, and nontoxic properties of the gelatin make it as one of the most useful biomaterial in the fabrication of controlled drug delivery systems [13]. Moreover, gelatin nanoparticles (GN) have been extensively used for the delivery of both hydrophilic and hydrophobic anticancer drugs such as cyclohexamide, doxorubicin, paclitaxel, and methotrexate [14–17]. A major benefit of GN for use in anticancer drug delivery is not only the very low cytotoxocity but also their simple and reproducible production that may lead to future upscaling. Moreover, the low cost of the base material, gelatin, makes this approach commercially attractive. However, intravenously injected GN are rapidly cleared from the systemic circulation by opsonization, C3-mediated uptake (initiated by complement activation) and preferential uptake of opsonized nanoparticles by the macrophages of the reticuloendothelial system (RES) [18]. But, poly(ethylene glycol) (PEG)-clouded GN (PEG-GN) have a longer circulation time and passive targeting potential to the tumor network and avoid protein binding, complement activation, and preferential uptake by the RES, which are discouraged by PEG chains [19]. The PEG-GN are then taken up by the tumor mass by enhanced permeation and retention effect [20]. Therefore, in the present investigation, an attempt was made to engineer NOS packed GN (NOS-GN) and NOS packed PEG-GN by optimizing the process variables. The pharmacokinetic profile was examined in experimental animals and in vitro cytotoxicity analysis was carried out on human breast cancer cell line (MCF7). Further,the structure of gelatin coacervates was elucidated with circular dichroism (CD).

Materials and methods

Materials

NOS [(3*S*)-6,7-dimethoxy-3-((5*R*)-5,6,7,8-tetrahydro-4-methoxy-6-methyl-1,3-dioxolo (4,5-*g*) isoquinolin-5-yl)-1(3*H*)-isobenzofuranone], gelatin (type B; bloom strength of approximately 225; 100–115 mmol/l of free carboxylic acid/100 g of protein with isoelectric point of 4.7–5.2, and average molecular weight of 40 000–50 000 Da), and 3-[4, 5-dimethylthiazol–2–yl]-2,5-diphenyl tetrazolium bromide (MTT) were purchased from Sigma (St Louis, Missouri, USA). Monomethoxy-PEG with a molecular weight of 5000 Da was obtained from Fluka Chemicals (New South Wales, Australia). Epichlorhydrin was procured from Spectrochem (Mumbai, India). Glutaraldehyde (GLA; 25% aqueous solution) was purchased from Loba Chemie (Mumbai, India). 2,4,6-Trinitrobenzene sulfonic acid (TNBS) was obtained as a gift sample. All other chemicals used were of analytical grade.

Analytical estimation of noscapine

Standard NOS (10 mg) was dissolved in 0.02 mol/l hydrochloric acid to make a 100-ml stock solution, of which different volumes were used to prepare the working solution. NOS showed a maximum absorption at 311.2 nm ($A_{311.2}$) scanned in an ultraviolet spectrophotometer (Shimadzu, Kyoto, Japan) [21]. The value of $A_{311.2}$ of the standard NOS solutions was used to produce a plot of $A_{311.2}$ *vis-à-vis* the concentration of NOS, allowing the standard regression equation (1) in the range of $C = 10$–100 μg/ml.

$$y = 0.0065\,x + 0.0149,\ R^2 = 0.9983. \quad (1)$$

Synthesis and purification of poly(ethylene glycol)-epoxide

Monomethoxy-PEG (25 g; 5 mmol/l) was dissolved in 100 ml of *N*,*N*-dimethylformamide (dehydrated) containing triethanolamine (1% w/v) at 40°C for 4 h under constant stirring conditions by a magnetic stirrer. To this solution, a five times molar excess (2.31 g) of epichlorhydrin was added and the reaction continued overnight at room temperature under reflux conditions. The epoxide derivative so formed was precipitated in cold diethyl ether. The PEG-epoxide was then washed thrice with cold diethyl ether and dried *in vacuo* [18]. The percentage yield was calculated using equation (2):

$$\%\,\text{yield} = \text{Theoretical yield}/\text{Practical yield} \times 100 \quad (2)$$

Synthesis of poly(ethylene glycol)-grafted gelatin

PEG-epoxide and gelatin were dissolved in 20 ml of alkaline borate buffer [solution A (boric acid; 1.24 g/100 ml distilled water); solution B (sodium bicarbonate; 1.9 g/100 ml distilled water), mixed in the ratio of 8.5 : 1.5, pH 8.5] and the reaction for grafting PEG-epoxide to the primary amine groups of basic amino acids of gelatin was carried out for 14 h at 40°C. The mixture was precipitated in three-fold excess of acetone to remove any unreacted PEG-epoxide, washed with acetone, and dialyzed against deionized distilled water using a dialysis membrane (12–14 kDa; Sigma) for up to 24 h at 25°C and then lyophilized [CHRIST LT 105 equipped with CHRIST CT 02-50 (Osterode amHarz, Germany)] [18].

Determination of free amine groups

The free amine groups in PEG-grafted and ungrafted gelatin were determined by a 2,4,6-TNBS assay [22]. TNBS is a rapid and sensitive assay reagent for the determination of free amine groups. In brief, ungrafted gelatin and PEG-grafted gelatin (11 mg) were mixed with

Copyright © Lippincott Williams & Wilkins. Unauthorized reproduction of this article is prohibited.

a 1 ml of 4% sodium bicarbonate (pH 8.5) solution and 1 ml of 0.5% TNBS and heated at 40°C for 4 h with mild shaking. HCl (6 N, 3 ml) was then added and the mixture was heated at 70°C for 1 h to hydrolyze and dissolve any insoluble materials. The hydrolysate was then diluted with 5 ml of distilled water and extracted with diethyl ether. A 5-ml aliquot of the aqueous phase was removed from each sample and heated for 15 min in a hot water bath, cooled to room temperature, and diluted with 15 ml of distilled water. Absorbance was measured at 346 nm using an ultraviolet spectrophotometer (Shimadzu) against a blank. The experiment was carried out in triplicate. Blanks were prepared using the procedure described above, but HCl was added before TNBS to prevent a reaction between gelatin amine groups and TNBS.

Preparation of gelatin and poly(ethylene glycol)-grafted gelatin nanoparticles

NOS-GN were engineered by a two-step desolvation method [23]. In brief, 25 ml of gelatin solution (5% w/v) was prepared at room temperature. Gelatin was desolvated by adding 25 ml of acetone or ethanol dropwise to precipitate the high molecular weight gelatin, and kept for sedimentation. The supernatant was discarded and the sediment was redissolved in 25 ml of water at a pH between 2 and 12 with 50 mg of NOS. Acetone or ethanol was again added dropwise to form nanoparticles. GN were further crosslinked with GLA (25% aqueous solution), the excess of which was neutralized by adding 500 mg of glycine. Purification was done by centrifugation (Multi 1 S-R centrifuge, Thermo Electron Corporation, Massachusetts, USA) at 8000*g* and the desolvating agent was removed by slow vaporization over 24 h. A similar method was adopted for the synthesis of NOS-PEG-GN.

Particle size and zeta potential analysis

Particle size and the zeta potential of nanoparticles (NOS-GN and NOS-PEG-GN) were determined by laser Doppler anemometry using a Zetasizer (Malvern Instruments, Worcestershire, UK). For particle size and ς potential analysis, 100 µl of the nanoparticle suspension (NOS-GN and NOS-PEG-GN) was dispersed in 4 ml of phosphate-buffered saline (PBS, 10 mmol/l; pH 7.4) and mean particle size and zeta potential were determined. An electric field of 150 mV was applied to observe the electrophoretic velocity of the nanoparticles. All the measurements were made at 25°C in triplicate.

Transmission electron microscopy

Particle shape and morphology were examined using transmission electron microscopy (Philips Morgagni 268, MD Eindhoven, The Netherlands) at a voltage of 80 kV. Aqueous dispersion of the nanoparticles (NOS-GN and NOS-PEG-GN) was drop cast onto a carbon-coated copper grid and the grid was air dried at room temperature before loading it on to the microscope.

Atomic force microscopy

The shape and surface morphology of NOS-GN and NOS-PEG-GN were also investigated using atomic force microscopy (AFM; Molecular Imaging, Arizona, USA). The images were captured in air using a 0.7 µm AFM head. The sample was placed on a xyz-piezo-translator (Arizona, USA) and scanned by using a sharp diamond tip that was mounted on a gold-coated 200 µm triangular Si_3N_4 microfabricated cantilever [Arizona, USA; force constant = 0.6 N/m). The force between the tip and the sample usually ranges from 10^{-7} to 10^{-9} N.

Electron spectroscopy for chemical analysis

GN and PEG-GN were analyzed with electron spectroscopy for chemical analysis (ESCA; KRATOS ESCA Model AXIS 165, Manchester, UK) to determine the elemental composition and identification of chemical functional groups of 100-Angstrom thick surface layers. The spectra were taken on a surface science instrument, x-probe spectrophotometer, with a monochromatized Al X-ray source (300 W). A 5 eV flood gun (Manchester, UK) was used to neutralize the surface charge. The surface elemental composition was determined by using standard Scofield photoemission cross sections [24]. Identification of chemical functional groups was obtained from the high-resolution peak analysis of carbon-1 s (C1 s), oxygen-1 s (O1 s), and nitrogen-1 s (N1 s) envelopes.

Circular dichroism

CD spectroscopy was carried out at 25°C with constant N_2 flushing using a CD instrument (Jasco J-715, Essex, UK). The far-ultraviolet CD spectra of gelatin proteins were measured from 190 to 250 nm in distilled water at pH 2.5. All measurements were taken 10 min after sample preparation with the following instrument setting: 0.5 s; scan speed, 200 nm/min; sensitivity 100 mdegree; and 1 nm spectra bandwidth. An average of three scans was taken. The final concentration of protein used in far-ultraviolet CD analysis was 1 mg/ml.

Nanoencapsulation efficiency

NOS-GN and NOS-PEG-GN (50 mg) were digested in 50 ml of 0.02 N HCl. The suspension was warmed for few minutes and was then kept undisturbed for 48 h and finally centrifuged at 8000*g*, filtered with a 0.2 µm membrane filter (MDI, Ambala, India), and an aliquot of the filtrate diluted appropriately with a solvent system, was analyzed at 311.2 nm [20] (Shimadzu) to determine the amount of NOS entrapped in nanoparticles. The experiment was performed in triplicate.

Fourier transform infrared spectroscopy

Fourier transform infrared (FTIR) spectroscopy was used as a technique to express any drug–polymer interaction during the fabrication of drug-loaded nanoparticles. The spectrum was recorded for NOS, GN, a physical mixture of NOS and GN and NOS-GN using Spectrum BX

Copyright © Lippincott Williams & Wilkins. Unauthorized reproduction of this article is prohibited.

(Perkin Elmer, Massachusetts, USA) infrared spectrophotometer. Samples were prepared in a KBr disk (2 mg sample in 200 mg KBr) with a hydrostatic press at a force of 40 psi for 4 min. The scanning range was 400–4400/cm and the resolution was 4/cm.

Powder X-ray diffraction analysis

Powder X-ray diffraction analysis (PXRD) was carried out to investigate the effect of the nanoencapsulation process on the crystal structure of the drug. PXRD patterns were recorded on a RIGAKU, Rotaflex, RV 200 (Rigaku Corporation, Tokyo, Japan) PXRD using Ni-filtered, CuK_{α} radiation at a voltage of 60 kV and a current of 50 mA. The scanning rate used was 1°/min over the 10–60° diffraction angle (2θ) range. The PXRD patterns of the NOS crystals, GN, physical mixture of NOS and GN, and NOS-GN were recorded.

In-vitro drug release kinetic experimentation

The kinetics of drug release from the dispersion of NOS-GN and NOS-PEG-GN were examined using the equilibrium dialysis technique, a method for the quantitation of drug transport across a dialysis membrane [25,26]. In brief, 2 ml of a drug-loaded nanoparticle suspension was put in the dialysis bag (12 kDa, Sigma) and was dialyzed against 250 ml of PBS (10 mmol/l at pH 4.5 and pH 7.4, respectively) [27] maintained at 37°C with a rotation speed of 50 rpm. At different time intervals, a sample of 5 ml was withdrawn and replaced with a fresh solvent to mimic infinite sink conditions. The NOS concentration in the sample was measured using an ultraviolet spectrophotometer (Shimadzu) at 311.2 nm [21]. Quantification of drug release was done using a mathematical model based on zero-order or first-order kinetic release of the drug from colloidal matrices [25], which accounts for the diffusion of the drug through a dialysis membrane into the external dissolution medium. In dynamic dialysis, the concentration of the drug in the dissolution (outside) medium was monitored as a function of time. The release kinetics was calculated using the mathematical model equation (3):

$$\ln\left[C_1 - Qm^{\circ}/V_T\right] = -k_M t + \ln[k_C Q_{M^{\circ}}/(k_M - K_{CV}) V_1 V_2] \quad (3)$$

where

C_1 is the concentration of the drug in the dialysate (outer solution),

Q_{M^0} is the total amount of drug associated with the nanoparticles at time 0,

k_M is the first-order release rate constant,

k_C is the apparent permeability constant of dialysis tubing,

V_1 and V_2 are volumes of solution outside and inside the dialysis bag $V_T = V_1 + V_2$, and

$$K_{CV} = k_C V_T / V_1 V_2$$

Stability study on storage

The ability of GN and PEG-GN to retain NOS was assessed by keeping the optimized formulations in sealed vials (10 ml capacity) after flushing with nitrogen at 4 ± 0.5, 25 ± 0.5, and 37 ± 0.5°C for 3 months under controled conditions and then evaluated for their size and leak percentage of encapsulated NOS at 311.2 nm.

Pharmacokinetic analysis

Pharmacokinetic analysis of NOS, NOS-GN, and NOS-PEG-GN was carried out as per our earlier published method using high-performance liquid chromatography for the determination of NOS in plasma samples [6,7]. The high-performance liquid chromatography system consisted of Shimadzu instruments equipped with a Shimadzu LC-10 A pump and an SPD-10Avp (diode array; Shimadzu, Kyoto, Japan) detector. The analytical column used was LiChrospher @ 60 RP select-B (C8; Merck, Darmstadt, Germany) reversed-phase column (4×125 mm) packed with 5 μm particles. The column temperature was equivalent to room temperature (25°C). The mobile phase consisted of ammonium acetate:acetonitrile (65 : 35); 20 mmol/l ammonium acetate solution was adjusted up to pH 4.5 using glacial acetic acid. The solution was filtered and degassed by vacuum filtration through a 0.22 μm membrane filter (MDI) before use and was freshly prepared for each run. The flow rate of the mobile phase was adjusted to 1 ml/min. The wavelength of detection was 232 nm and the detector was set at 0.005 absorbance unit, full scale. The pharmacokinetic study was carried out following the guidelines of Committee for the Purpose of Control and Supervision of Experiments on Animals, Ministry of Culture, Government of India. Swiss female albino mice weighing 20–30 g were maintained on standard laboratory chow and water *ad libitum* in a temperature-controlled and light-controlled environment at the Hindu College of Pharmacy, Sonepat, Haryana, India. Eighty-one female mice were randomly divided into 27 groups of three animals each corresponding to the time points of blood collection. Although this gives us three mice per time point for analysis, but to ensure that our systemic error is acceptable we analyzed each sample in triplicate and saw no variation (at 95% confidence level). NOS and NOS equivalent to 50 mg/kg in NOS-GN and NOS-PEG-GN were administered intravenously through the tail vein. Plasma levels of NOS were monitored for 12 h. Samples were collected at 0, 0.016, 0.083, 0.25, 0.5, 1, 2, 3, 4, and 12 h in all groups. Approximately 750 μl of blood was collected from the retro-orbital vein into polypropylene microcentrifuge tubes containing 25 μl of 20 mmol/l sodium citrate.

Copyright © Lippincott Williams & Wilkins. Unauthorized reproduction of this article is prohibited.

The blood samples were centrifuged at 4600 rpm for 15 min at 4°C and the plasma was separated. Plasma samples were stored at −80°C until analyzed. Plasma concentration data were analyzed with standard non-compartmental methods using WINNONLIN (Software version 4.1; Pharsight, California, USA). Composite plasma concentration–time profiles were constructed for female mice. The following pharmacokinetic parameters were assessed: k_e (/h), $t_{1/2}$ (h), AUC_{last} (h μg/ml), AUC_{inf} (h μg/ml), area under first moment curve (AUMC) (h^2 μg/ml) MRT (h), total body clearance (CL_{total}) (l/h), volume of distribution (l). The area under the curve was calculated by the linear trapezoidal rule up to the last sampling point (AUC_{last}) with detectable levels with extrapolation to infinity (AUC_{inf}) by equation (4),

$$AUC_{last} + C/k_e \quad (4)$$

where k_e represents the elimination rate constant; k_e was calculated from the slope of the data points in the final log-linear part of the drug–concentration time curve by weighted least square linear regression analysis. The terminal disposition half-life ($t_{1/2}$) value was calculated using equation (5),

$$t_{1/2} = 0.693/k_e \quad (5)$$

Mean residence time (MRT) can be calculated from the AUC_{last} and AUMC. AUMC is obtained from a plot of the product of plasma drug–concentration and time vis-à-vis t from zero to infinity.

$$MRT = AUMC/AUC_{last} \quad (6)$$

Similarly, volume of distribution can be calculated from CL_{total}/k_e, where CL_{total} = dose/$AUC_{infinite}$.

Cytotoxicity analysis

The MCF-7 was maintained as monolayers at 37°C in 25 cm^2 tissue culture flasks (Tarsons, India) using Dulbecco's modified Eagle's medium (Sigma) supplemented with 5% fetal calf serum (Biologicals, Israel). Cells were passaged routinely in the exponential growth phase twice a week using 0.05% trypsin–EDTA solution in PBS (pH 7.4) for trypsinization. All experiments were carried out with asynchronously growing cells in the exponential growth phase (24 h after plating). Cytotoxicity was determined by MTT assay using a 96-well microtiter plate. Three thousand cells per well were plated in 200 μl of the complete medium and treatment with these ligands was carried out. For determining the percentage of survival, cells were exposed continuously with varying concentrations of NOS, NOS-GN, and NOS-PEG-GN for 3 days. At the end of the treatment, control and treated cells were incubated with MTT at a final concentration of 0.5 mg/ml for 2 h at 37°C and the medium was removed. The cells were lysed and the formazon crystals were dissolved using 100 μl dimethylsulfoxide. The absorbance was read at 570 nm using 630 nm as the reference wavelength using an enzyme-linked immunosorbent assay reader (Tecan).

Statistical analysis

The results are expressed as the mean ± standard deviation for $n \geq 3$. Statistical significance was determined with one-way and two-way analyses of variance (ANOVA) tests. A P value of less than 0.05 was taken as a significant level of difference.

Results and discussion

Characterization of poly(ethylene glycol)-grafted gelatin

The percentage of free amine groups of gelatin that were reacted with PEG-epoxide (86% yield) in the modified gelatin derivative was determined by TNBS assay as a function of the amount of PEG-epoxide added per gram of gelatin (Table 1). With increasing amounts of PEG-epoxide, there was an increase in the percentage of amine groups that were modified by PEG. In this investigation, we used the sample PEG-E 2 (35 ± 4.3% blocked amine groups of gelatin) for the fabrication of NOS-PEG-GN as higher PEG-derivatized gelatin samples create difficulty in the production of PEG-GN of optimum size.

Characterization of nanoparticles

Transmission electron microscopy and atomic force microscopy

The transmission electron microscopy and AFM micrographs of the lyophilized NOS-GN and NOS-PEG-GN (Fig. 1) corroborated that the nanoparticles were smooth and spherical in shape. The photomicrographs also indicated that centrifugal force and freeze-drying factors did not affect nanoparticle texture. Most peripheral human tumor vessels have a permeability cut-off of less

Table 1 Percentage of amine groups of gelatin modified with PEG-epoxide

Sample code	Amount of PEG-epoxide (gm)	Amount of gelatin (gm)	Amine groups modified (%)[a]
PEG-E1	0.2	1.0	20 ± 2.5
PEG-E2	0.6	1.0	35 ± 4.3
PEG-E3	1.0	1.0	54 ± 5.1
PEG-E4	1.4	1.0	62 ± 1.9
PEG-E5	1.8	1.0	71 ± 4.3
PEG-E6	2.2	1.0	76 ± 3.2

PEG-E, poly(ethylene glycol) epoxide.
[a]Values are shown as mean ± standard deviation for $n \geq 3$.

Copyright © Lippincott Williams & Wilkins. Unauthorized reproduction of this article is prohibited.

Fig. 1

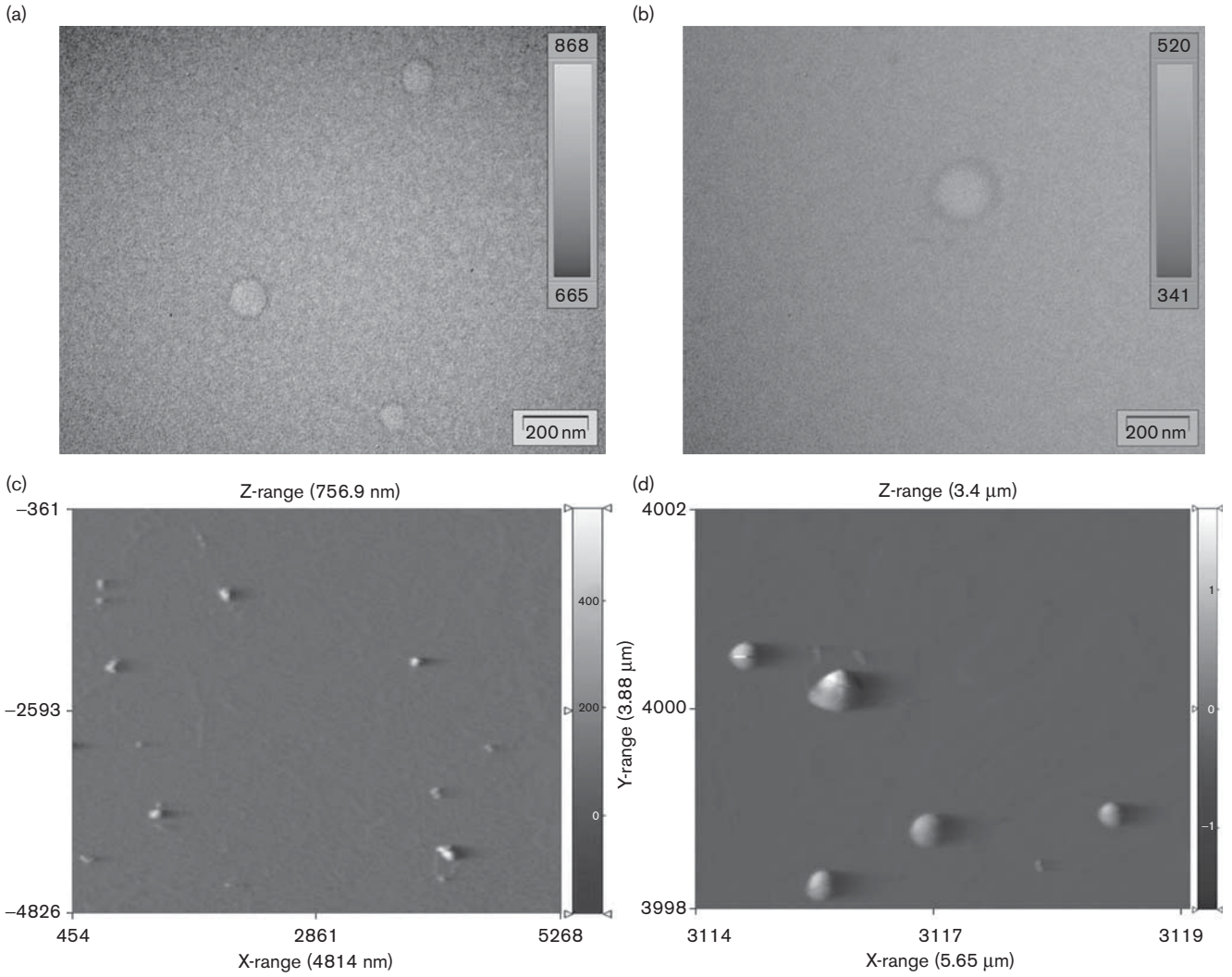

Transmission electron micrograph of (a) noscapine-loaded gelatin nanoparticles (NOS-GN), (b) noscapine-loaded poly(ethylene glycol)-grafted gelatin nanoparticles (NOS-PEG-GN). The scale bar represents a distance of 200 nm. Atomic force microscopy of (c) NOS-GN (d) NOS-PEG-GN.

than 600 nm [20]. NOS-GN and NOS-PEG-GN, therefore, may provide an effective means of NOS delivery to solid tumors after intravenous or intratumoral administration of the formulations in future in-vivo studies.

Electron spectroscopy for chemical analysis

ESCA analysis shows the high-resolution –C–H– (hydrocarbon), –C–O– (ether) and –C = O– (carbonyl) peaks in the C1 s envelope of the GN and the PEG-GN at their characteristic binding energies of 284.602, 286.151, and 287.587 eV, respectively (Fig. 2). The surface presence of PEG chains in the PEG-GN sample was confirmed by comparing the high-resolution ESCA spectra of the modified gelatin sample with unmodified gelatin sample. The observed increase in the relative peak intensity of the ether peak in the PEG-grafted gelatin derivative (from 47.7% in the gelatin sample to 57.8% in the PEG-grafted gelatin) is consistent with the presence of ethylene oxide residues of PEG on the surface of the modified gelatin derivative.

Evaluation of various process variables

In this investigation, we studied the effect of various processes and formulation parameters on the production of NOS-GN. It has been widely accepted that nanoparticles have 2.5-fold greater uptake in a caco-2 cell line in comparison with microparticles [28]. However, systemically administered nanoparticles are rapidly cleared from the circulation by a process of opsonization, which is initiated by complement activation and preferential uptake of the nanoparticles by the organs of RES. Therefore, to increase their systemic circulation time, they need to be protected from RES. Earlier studies also showed that particle size significantly affects cellular and

Copyright © Lippincott Williams & Wilkins. Unauthorized reproduction of this article is prohibited.

tissue uptake, and in some cell lines, only the submicron size particles are taken up efficiently than the larger size microparticles [28,29]. Therefore, it is necessary to control the size of nanoparticles to achieve cellular targeting. We observed that numerous changes in the pH of gelatin aqueous solution have greater effect on nanoparticle size. There was significant (one-way ANOVA; $P < 0.05$) increase in particle size from samples GN1–GN3 (127 ± 15–173 ± 17 nm), when the pH of the aqueous gelatin solution was increased from 2.5 to 7.4, keeping other variables constant (Table 2). The isoelectric point of gelatin B is approximately 4.5. The pH of the gelatin solution after the desolvation step and before crosslinking with GLA is brought to 2.5 units by adding 0.1 mol/l HCl; the resultant positive NH_3^+ group becomes predominant to facilitate crosslinking with –CHO groups of GLA and produces smaller particles at pH 2.5 and bigger particles at pH 7.4 [30]. In contrast, the pH of the dispersion medium changes the nanoparticle size in a reverse manner when incubated for 24 h at pH values of 4.5 and 7.4 (Table 3). As the pH of the dispersion medium increased from 4.5 to 7.4, the nanoparticle size decreased from 195 ± 13.5 to 150 ± 10.2 nm while other variables were kept constant. It was reported that increasing or decreasing the pH from the isoelectric point of gelatin would cause net negative or positive charges because of the ionization of COOH and NH_2 groups, respectively. Addition of a base affects the carboxyl groups only as the amine groups are crosslinked with GLA. It may (i) ionize the COOH groups further and enhance electrostatic repulsion, or (ii) increase the ionic strength and weaken the electrostatic repulsion. At low pH, these two effects partially negate each other. At some threshold pH when all the COOH groups are ionized, further addition of a base can only enhance the second effect, which explains the contraction of the particle at a pH of 7.4. Thus, we have observed that there is a decrease in the nanoparticle size as the pH increases [31]. The maximum nanoencapsulation efficiency of GN (GN1) was found to be $65.32 \pm 3.81\%$ with a ς potential of -39.3 ± 0.4 mV as shown in Table 2. When the drug was encapsulated in PEG-GN (GN8), it showed an entrapment efficiency of $63.65 \pm 1.61\%$ with a significant (two-way ANOVA; $P < 0.05$) decrease in the negative surface charge of -30.2 ± 0.6 mV. The decrease in the ς potential value of NOS-GN to NOS-PEG-GN corroborates the presence of PEG brush on the GN. Moreover, negative ς potential further prevents agglomeration

Fig. 2

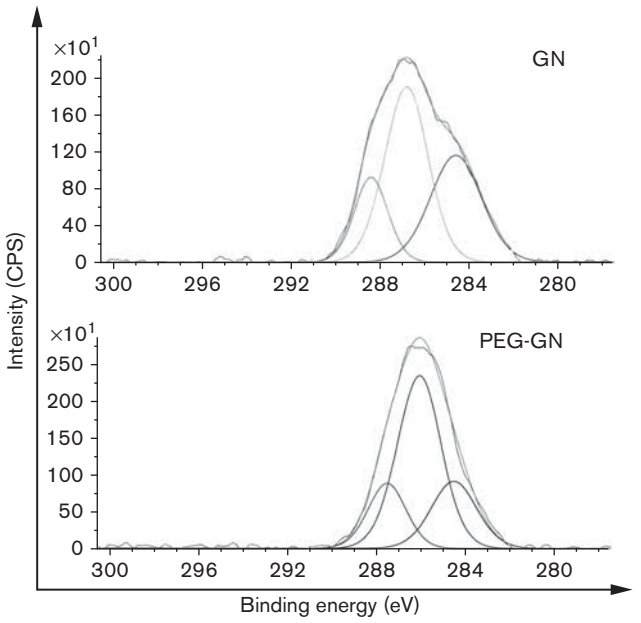

Nanoparticle sample	Relative peak area (%) –C–H– (284.602)	–C–O– (286.151)	–C=O– (287.587)
GN	34.4	47.7	17.9
PEG-GN	23.4	57.8	18.8

High-resolution C1 s scans of electron spectroscopy for chemical analysis for the surfaces of gelatin-grafted and polyethylene-grafted gelatin. The scans show the peak intensities of the species –C–H– (hydrocarbons), –C–O– (ether), and –C=O– (carbonyl) groups at 284.602, 286.151, and 287.587 eV, respectively. The percentage of –C–O– peak area for each spectrum is provided. GN, gelatin nanoparticles; PEG-GN, poly(ethylene glycol)-grafted gelatin nanoparticles.

Table 2 Effect of desolvating agent, pH, temperature, and glutaraldehyde concentration on the particle size (measured at pH 7.4) and nanoencapsulation efficiency

Sample code	pH	Desolvating agent	Temp (°C)	GLA Conc. (μl)	Size[a] (nm)	Polydispersity index[a]	NE (%)[a]	Zeta potential (mV)[a]
GN1	2.5	Acetone	40	250	127 ± 15	0.095 ± 0.026	65.32 ± 3.81	−39.3 ± 0.4
GN2	4.5	Acetone	40	250	146 ± 20	0.081 ± 0.009	57.81 ± 2.32	–
GN3	7.4	Acetone	40	250	173 ± 17	0.085 ± 0.065	33.32 ± 6.45	–
GN4	2.5	Ethanol	40	250	281 ± 10	0.057 ± 0.010	59.45 ± 4.32	–
GN5	2.5	Acetone	60	250	282 ± 16	0.083 ± 0.011	57.31 ± 2.21	–
GN6	2.5	Acetone	40	400	120 ± 25	0.120 ± 0.071	56.45 ± 2.28	–
GN7	2.5	Acetone	40	500	121 ± 13	0.088 ± 0.067	58.41 ± 1.12	–
GN8[b]	2.5	Acetone	40	250	203 ± 10	0.052 ± 0.074	63.65 ± 1.61	−30.2 ± 0.6

Conc., concentration; GLA, glutaraldehyde; GN, gelatin nanoparticles; NE, nanoencapsulation efficiency; Temp, temperature.
[a]Values are shown as mean ± standard deviation for $n \geq 3$.
[b]Poly(ethylene glycol)-GN.

Copyright © Lippincott Williams & Wilkins. Unauthorized reproduction of this article is prohibited.

Table 3 Effect of pH on the size of gelatin nanoparticles (GN1) incubated in phosphate buffer saline (pH 7.4) for 24 h

pH	Size of gelatin nanoparticles (nm)[a]
4.5	195 ± 13.5
7.4	150 ± 10.2

[a]Values are shown as mean ± standard deviation for $n \geq 3$.

of the nanoparticles. Temperature also influences nanoparticle size. Increase in temperature from 40 to 60°C (GN1 and GN5) also significantly (two-way ANOVA; $P < 0.05$) increased the particle size from 127 ± 15 to 282 ± 16 nm, which might be attributed to the gelling properties of gelatin. In solution, the triple helical structure begins to uncoil because of an increase in temperature and thus decreases viscosity. At 40°C, the chains seem to be sufficiently uncoiled and the addition of the desolvating agent causes a better-controlled precipitation of the macromolecules compared with higher temperature. Moreover, acetone or ethanol as a desolvating agent also influences nanoparticle size as shown in Table 2. It was observed that acetone produced smaller nanoparticles (GN1; 127 ± 15 nm) in comparison with ethanol (GN4; 281 ± 10 nm) while keeping the other variables constant (40°C; 250 µl GLA). This fact has also been elucidated with CD spectroscopy, as it is an effective approach to investigate the secondary structural features of protein in solution. Figure 3a shows the CD spectra of aqueous gelatin solution (1 mg/ml) without pH adjustment and aqueous gelatin solution (1 mg/ml) at pH 2.5. The data show a peak at λ of approximately 200–210 nm and dip at λ of approximately 230 nm consistently for both solutions. It is known that unless an unusual fraction of aromatic amino acid is present, optical activity in the region with λ of approximately 190–230 nm is dictated by the peptide backbone of proteins. Moreover, this region is devoid of any aliphatic side chain contributions. Therefore, it allows the structural description of the polypeptide backbone to be expressed as a weighted linear sum of contributions from α-helix, β-turns, and random coils. Figure 3b also shows a somewhat similar CD profile when aqueous gelatin solution (1 mg/ml; pH 2.5) is titrated with ethanol. It also shows a peak at 210 nm and a dip at 230 nm. This might be attributed to the fact that gelatin is a weak polyampholyte having positively and negatively charged segments. Addition of ethanol facilitates the process of inducing chain collapse and positively charged segments interact with negatively charged segments. Charge neutralization of polyion segments precedes phase separation and the polyions do not precipitate out of the solvent. Addition of ethanol allows rupture of hydrogen bonds between water molecules and the polyion. However, the water molecules bind selectively with ethanol molecules through hydrogen bonding and the resultant binary mixture becomes a marginal solvent for gelatin molecules. This results in the reduction of the overall spatial extension of the polyelectrolyte chain, thereby bringing the complementary charged segments closer. This leads to self-charge neutralization and formation of gelatin particles in a single chain, which are mostly present in the supernatant; simultaneously, intermolecular segments of complementary charge form aggregates. As these aggregates may not be fully charge-neutralized, they can attract other gelatin molecules and thus grow in size. Moreover, the dielectric constant of the gelatin aqueous solutions also falls as ethanol volume increases facilitating stronger electrostatic interaction and hence, growth in aggregate size, which drives the system toward coacervation [32]. In contrast, Fig. 3c shows the CD data of aqueous gelatin solution (1 mg/ml; pH 2.5) titrated with acetone. The spectra indicated that α-helical contents of gelatin are no longer present in gelatin aqueous solution titrated with

Fig. 3

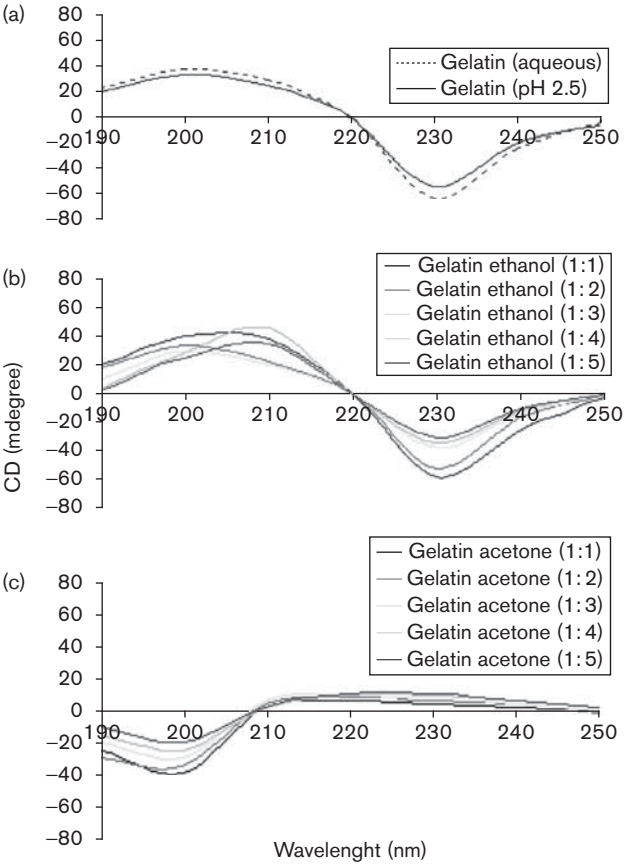

Circular dichroism (CD) curves of (a) aqueous gelatin solution (1 mg/ml; without pH adjustment) and aqueous gelatin solution (1 mg/ml; pH 2.5). (b) Aqueous gelatin solution (1 mg/ml; pH 2.5) titrated with different aliquots of ethanol. (c) Aqueous gelatin solution (1 mg/ml; pH 2.5) titrated with different aliquots of acetone. Results indicated that decrease in pH from its isoelectric point (4.7–5.2) to pH 2.5 retains the secondary structural characteristics of gelatin. Moreover, titration with aliquots of ethanol promotes the formation of gelatin nanocoacervates but still retains the α-helical contents of gelatin. However, titration with acetone as a desolvating agent causes the formation of random coils and forms the compact mass in gelatin nanocoacervates.

Copyright © Lippincott Williams & Wilkins. Unauthorized reproduction of this article is prohibited.

acetone as no dip was observed at 230 nm, which is the characteristic band of α-helix. This represents the formation of random coils in acetone-mediated coacervate formulation. Acetone decreases the dielectric constant of water as acetone is a nonpolar solvent and causes the formation of random coils in gelatin secondary structure. This does not allow the positively charged segments to bind to negatively charged segments, and thus does not allow the formation of large aggregates and reduces the nanoparticle size.

Increasing the concentration of GLA from 250 to 500 µl (GN1; 127 ± 15 nm, GN6; 120 ± 25 nm, GN7; 121 ± 13 nm) did not show any significant change (one-way ANOVA; $P > 0.05$) in the nanoparticle size as shown in Table 2. Stability study also assures that 4 and 25°C are the optimum temperatures (Table 4) to store NOS-GN (GN1) and NOS-PEG-GN (GN8).

Fourier-transform infrared spectroscopy

FTIR spectra were recorded to analyze the structure of any new chemical linkage formed during the encapsulation of NOS in the nanoparticle matrix. The FTIR spectrum peaks of NOS, GN, physical mixture of NOS and GN, and NOS-GN are shown in Table 5. The assignment of FTIR scans indicates that NOS exhibited its characteristics peak at 1755/cm, indicating the presence of an intact and stable lactone ring. Other peaks of NOS that were observed are 2985/cm (–C = O stretching vibrations), 2944, 2882, 2842, 2798/cm due to various $–OCH_3$ and $–CH_3$ groups. The spectrum of blank GN shows the characteristic protein backbone at 1540–1650/cm (multipeak absorption pattern, typical of protein backbone) and 1462/cm (vibrational, aldimine stretching, crosslinking of gelatin). These peaks were almost unchanged in NOS-GN except suppression of the peak at 1755/cm, which indicates stability, and the presence of NOS in GN. These studies corroborate that there is no significant interaction between NOS and GN.

Powder X-ray diffraction pattern

We next attempted to define the crystal structure of NOS in GN using the PXRD technique. The PXRD pattern of NOS showed peaks that were intense and sharp indicating its crystal structure (Fig. 4a–d). Even GN also possesses few sharp peaks of low intensities. Therefore, a physical mixture of NOS and GN showed undefined broad, diffused peaks with low intensities. Although this signifies an amorphous structure, a few sharp peaks having less intensity were also observed. Finally, NOS-GN prepared by the desolvation method showed peaks of diminished intensity, which indicated that the crystal structure of NOS deformed to the amorphous state. The amorphous state because of the absence of an ordered crystal lattice requires minimal energy and thus provides the maximal solubility advantage to further enhance the bioavailability of poorly water-soluble drugs. However, limitations of amorphous systems such as physical instability and higher chemical reactivity act as a hurdle in their extensive commercialization. Polymers are usually used to provide an amorphous matrix in which the drug can dissolve, whereby the viscosity of the matrix is usually high enough to prevent recrystallization on storage. The X-ray diffraction pattern of NOS-GN showed that nanoparticles recovered as fine dry powder in the form of a molecular dispersion, providing intimate contact between the components, thus generating a stable form even under accelerated stability conditions.

Table 4 Storage stability study of noscapine-loaded gelatin nanoparticles and noscapine-loaded poly(ethylene glycol)-grafted gelatin nanoparticles conducted for 3 months at different temperatures

	Storage temperature (3 months)		
Parameters	4 ± 0.5°C	25 ± 0.5°C	37 ± 0.5°C
Size[a]			
NOS-GN (GN1)	127 ± 15	130 ± 20	153 ± 11
NOS-PEG-GN (GN8)	203 ± 10	199 ± 13	220 ± 10
Nanoencapsulation efficiency[a]			
NOS-GN (GN1)	65.32 ± 3.81	64.43 ± 5.24	51.32 ± 4.56
NOS-PEG-GN (GN8)	63.65 ± 1.61	61.65 ± 3.51	53.55 ± 2.25

NOS-GN, noscapine-loaded gelatin nanoparticles; NOS-PEG-GN, noscapine-loaded poly(ethylene glycol)-grafted gelatin nanoparticles.
[a]Values are shown as mean ± standard deviation for $n \geq 3$.

Table 5 Assignment of FTIR spectrum of noscapine, blank gelatin nanoparticles, physical mixture of noscapine and blank gelatin nanoparticles, and noscapine-loaded gelatin nanoparticles

Infrared peaks	Functional groups	Sample
NOS	2985/cm	*v*, –C=O–
	2944, 2882, 2842, 2798/cm	*v*,–OCH_3/OCH_2
	1755/cm	*v*, lactone ring
	1425, 1388/cm	*v*, N–CH_3
GN	3549/cm	*v*, N–H stretching of CONH–,
	2932/cm	*v*, C–H stretching
	1646/cm	*v*, –C=O–
	1540–1650/cm	Multipeak absorption pattern, typical of protein backbone
	1462/cm	*v*, Aldimine stretching, crosslinking of gelatin
Physical mixture (NOS and GN)	2944, 2882, 2842, 2798/cm}	*v*,–OCH_3/OCH_2
	1755/cm	*v*, lactone ring
	1478/cm	*v*, Aldimine stretching, crosslinking of gelatin
NOS-GN	3384/cm	*v*,–OH
	2943/cm	*v*,–OCH_3/OCH_2
	1755/cm	*v*, lactone ring
	1478/cm	*v*, Aldimine stretching, crosslinking of gelatin

GN, gelatin nanoparticles; NOS, noscapine; NOS-GN, noscapine-loaded gelatin nanoparticles; *v*, vibrational.

In-vitro release kinetics

Release kinetics of noscapine from gelatin nanoparticles

Release of drug from the dialysis membrane/bag depends on the permeability constant, which was determined by adding a known quantity of drug (25 mg/ml) inside the dialysis bag and then monitoring the drug concentration

Copyright © Lippincott Williams & Wilkins. Unauthorized reproduction of this article is prohibited.

in the outer solution (C_1) as a function of time. Using the equation for permeability constant, that is, ln [Qm°-C_1 ($V_1 + V_2$)] = ln Qm° – K_{CV} t, a plot of ln [Qm°-C_1 ($V_1 + V_2$)] vis-à-vis time gives the slope equal to K_{CV}, which is found to be equivalent to approximately 0.0146/h/ml. The intercepts on the axis give the value of the original amount present inside the dialysis bag, which is approximately 24.8 mg, almost equal to the original amount showing that adsorption of the drug by the dialysis membrane was negligible. The drug release kinetics from GN depends on the rate of water uptake, drug dissolution/diffusion rate, and polymer glass–rubbery transition including matrix erosion or degradation rate. A representative graph of release kinetics of the drug from GN1 is shown in Fig. 5a. Drug release is found to follow a first-order release kinetic at pH 4.5. A plot of ln [C_1-Qm°/V_T] vis-à-vis time t for GN1 at pH 4.5 shows a biphasic release of the drug. Release rate constants for two phases were given by the slopes and are presented in Table 6. The initial (or first phase) release rate constant is greater than the terminal (or second phase) release rate constant showing that both the surface adsorbed (free drug) and the entrapped drug were released in the first phase, whereas only the entrapped drug was released in the second phase. The amount of drug released in both the phases was calculated using rate constant values and the percentage of release was calculated.

Fig. 4

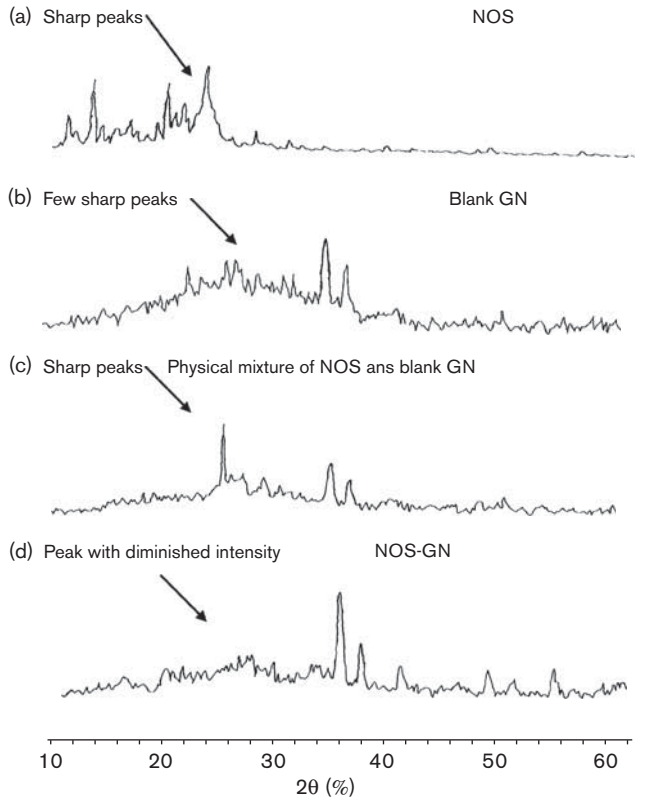

X-ray diffraction patterns of (a) noscapine (NOS), (b) blank gelatin nanoparticles (GN), (c) physical mixture of NOS and GN, (d) noscapine-loaded gelatin nanoparticles (NOS-GN). Suppression of peaks in NOS-GN indicated the amorphization of the NOS, which enhanced the wettability of the drug in the aqueous phase.

Fig. 5

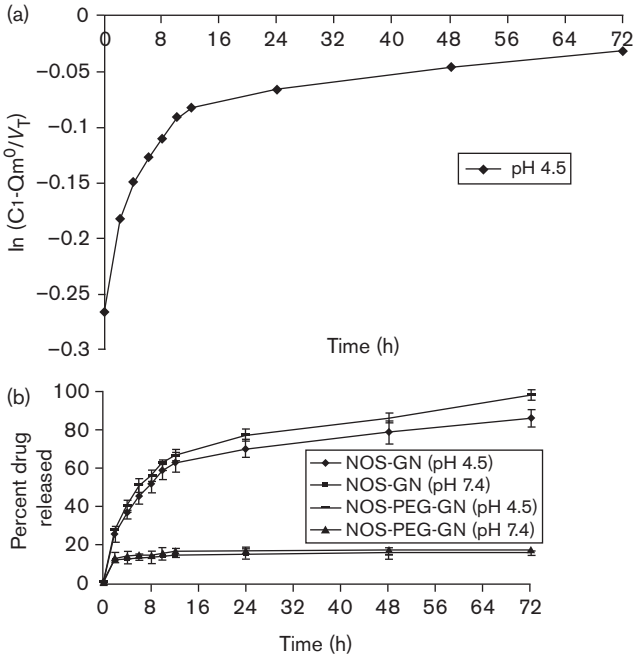

(a) Release kinetic profile of noscapine (NOS) from gelatin nanoparticles (GN) in different phases with release rate constants, (b) *in-vitro* release kinetics of NOS from GN (GN1) and poly(ethylene glycol)-grafted gelatin nanoparticles (PEG-GN) (GN8) at pH 4.5 and 7.4. Results documented that PEG-GN releases 97.28 ± 1.1% of NOS whereas GN releases 85.1 ± 4.2% of NOS at pH 4.5. This release is significantly ($P < 0.05$) higher than the NOS released (PEG-GN: 17.1 ± 1.2%; GN: 15.3 ± 2.7%) at pH 7.4. Values are shown as mean ± standard deviation for $n \geq 3$.

Effect of pH on in-vitro release

NOS has limited solubility in PBS (pH 7.4; 4.76 mg/l) [6]. Therefore, PBS (pH 7.4) cannot be considered as an ideal dissolution medium to study the dissolution profile of NOS-GN and NOS-PEG-GN. The pKa of an ionizable drug candidate is very important because it can be used to predict solubility, lipophilicity, and permeability at different pH; therefore, it helps to improve drug absorption by selecting a suitable pH. Drugs in solution are distributed between their neutral and charged forms on the basis of pH and pK_a. NOS has a pK_a of 7.8, which indicates that it is a weak base and is soluble only in acidic pH [5]. Therefore, we have considered pH 4.5 and pH 7.4 to study the in-vitro release profile of NOS-GN and NOS-PEG-GN. The effect of pH on in-vitro release of NOS from NOS-GN (GN1) and NOS-PEG-GN (GN8) is expressed in Fig. 5b. Data analysis indicated that NOS-PEG-GN (GN8) prepared with 250 µl of GLA,

Copyright © Lippincott Williams & Wilkins. Unauthorized reproduction of this article is prohibited.

Table 6 ***In vitro*** **release kinetics of noscapine from gelatin nanoparticles at pH 4.5 measured using mathematical model based upon zero-order or first-order kinetic release, as a function of time**

Sample (GN)	pH	NE (%)[a]	Release rate constants ($k_{m,1}$, $k_{m,2}$, k_m) (mg/h)	Initial drug release (%)	Terminal drug release (%)	Total drug release (%)
GN1	4.5	65.32 ± 3.81	8.33×10^{-3}, 7.19×10^{-4}, 7.611×10^{-3}	69.5	15.6	85.1

GN, gelatin nanoparticles; $k_{m,1}$, initial rate constant (release of entrapped + free drug); $k_{m,2}$, terminal rate constant (release of entrapped drug); k_m, $k_{m,1}-k_{m,2}$ (rate constant for the release of free drug); NE, nanoencapsulation efficiency.
[a]Values are shown as mean ± standard deviation for $n \geq 3$.

release 55.26% of NOS in PBS of pH 4.5 in the initial 8 h in comparison with 51.2% of NOS released by NOS-GN (GN1) at the same time interval. However, NOS-PEG-GN (GN8) releases only 14.53% of the drug at pH 7.4, which is significantly ($P < 0.05$) different from NOS release at pH 4.5. Similarly, NOS-GN releases 85.1 ± 4.2% of NOS at 72 h, which is significantly ($P < 0.05$) different from NOS-PEG-GN, which releases 97.28 ± 2.8% of NOS at 72 h at pH 4.5. For efficient systemic delivery of anticancer agents to solid tumors, they must be able to transfer through the circulatory system and reach the tumor mass in sufficient concentration, get transported across the microvessels, and diffuse into the interstitial space. Unfortunately, the irregular blood supply, high interstitial pressure, low pH and hypoxia, and lack of lymphatic system contribute to inefficient drug uptake and distribution in the tumor mass after systemic administration. The problem of optimum drug delivery to tumors is further compounded by newer generations of anticancer drugs, which have very poor diffusional properties. Hydrostatic pressure inside the tumor mass is significantly higher than in the vasculature. On account of the pressure gradient, anti-cancer drugs administered in the systemic circulation cannot diffuse evenly within the tumor mass. In addition, the tumor metabolic profile is different owing to poor perfusion resulting in elevated levels of lactic acid, and hence, a reduction in pH. As observed, GN releases higher amounts of NOS in an acidic environment (pH 4.5) and lower amounts of drug in physiological conditions (pH 7.4); this may potentially be targeted to the tumor cells [33]. Thus, NOS-PEG-GN might have the potential to efficiently deliver high therapeutic concentration within the solid tumor mass at low pH values. Thus, we have presented here that NOS-PEG-GN (GN8) are able to prevent the ionization of NOS because of controlled release from gelatin nanomatrix and increases the proportion of unionized drug at the tumor site, thereby improving the therapeutic efficacy of the drug [10].

Fig. 6

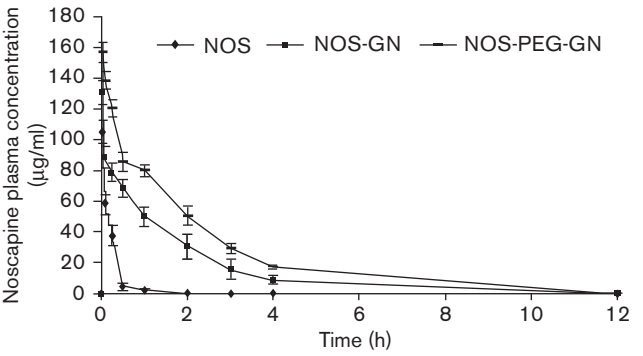

Comparative plasma concentration–time profile curves of noscapine (NOS), noscapine-loaded gelatin nanoparticles (NOS-GN) (GN1), and noscapine-loaded poly(ethylene glycol)-grafted gelatin nanoparticles (NOS-PEG)-GN (GN8) at the dose of 50 mg/kg injected intravenously in female Swiss albino mice. Values are shown as mean ± standard deviation for $n \geq 3$.

Pharmacokinetic analysis

The plasma concentration–time profiles of NOS, NOS-GN, and NOS-PEG-GN were compared at a single-dose level (50 mg/kg) in female mice on intravenous administration. As investigations indicated that NOS has intravenous LD_{50} dose of 83 ± 6.1 mg/kg [34], in this investigation, 50 mg/kg equivalent of NOS, NOS-GN (GN1), and NOS-PEG-GN (GN8) were administered intravenously in female mice and the plasma-concentration time profile curve was plotted as shown in Fig. 6. The main differences in the profiles of the fall in the plasma concentration of NOS vis-à-vis time for the three formulations lay in the significantly greater NOS recovery in the plasma for the NOS-PEG-GN over the NOS-GN and NOS. This increase in the dose recovered for the NOS-PEG-GN was seen for up to a total period of 4 h after which there were no significant ($P < 0.05$) differences in the plasma concentrations of the three formulations. The greater recovery of the concentration of NOS in the plasma with NOS-PEG-GN compared with NOS-GN and NOS was indicative of the long, circulating property of NOS-PEG-GN. NOS-PEG-GN were probably capable of avoiding both complement activation, recognition, and uptake by the components of RES. Surface PEG modification was found to prevent RES uptake for as long as 4 h after which NOS-PEG-GN probably were digested by serum proteases and the steric repulsion effect of surface PEG chains was not significant. Moreover, various parameters such as the elimination rate constant, half-life, MRT, volume of distribution, CL_{total}, and AUC for the three formulations in plasma are reported in Table 7. A relatively smaller elimination rate constant was observed in comparison with NOS and NOS-GN, which corresponds to a greater bioavailability of NOS-PEG-GN. Notable in these results are the

Copyright © Lippincott Williams & Wilkins. Unauthorized reproduction of this article is prohibited.

Table 7 Comparative pharmacokinetic parameters of noscapine, noscapine-loaded gelatin nanoparticles, and noscapine-loaded poly(ethylene glycol)-grafted gelatin nanoparticles at the dose of 50 mg/kg injected intravenously in female Swiss albino mice

Parameters	NOS[a]	NOS-GN (GN1)[a]	NOS-PEG-GN (GN8)[a]
$-k_e$ (/h)	0.622 ± 0.02	0.276 ± 0.01	0.06 ± 0.01
$t_{1/2}$ (h)	1.11 ± 0.08	2.51 ± 0.10	11.55 ± 0.16
AUC_{last} (h μg/ml)	22.29 ± 4.58	203.94 ± 9.57	298.90 ± 7.78
AUC_{inf} (h μg/ml)	25.82 ± 1.36	235.38 ± 4.22	592.23 ± 3.21
AUMC (h μg/ml)	26.94 ± 4.59	501.04 ± 19.87	888.69 ± 15.47
MRT (/h)	1.20 ± 0.05	2.45 ± 0.15	2.97 ± 0.25
Vd (l)	3.11 ± 0.7	0.768 ± 0.009	1.4 ± 0.008
CL_{total} (l/h)	1.93 ± 0.11	0.212 ± 0.015	0.084 ± 0.004

AUC_{last}, area under the curve up to the last sampling point; AUC_{inf}, area under the curve with extrapolation to infinity; CL_{total}, total body clearance; MRT, mean residence time; NOS-GN, noscapine-loaded gelatin nanoparticles; NOS-PEG-GN, noscapine-loaded poly(ethylene glycol)-grafted gelatin nanoparticles; Vd, volume of distribution.
[a]Values are shown as mean ± standard deviation for $n \geq 3$.

Fig. 7

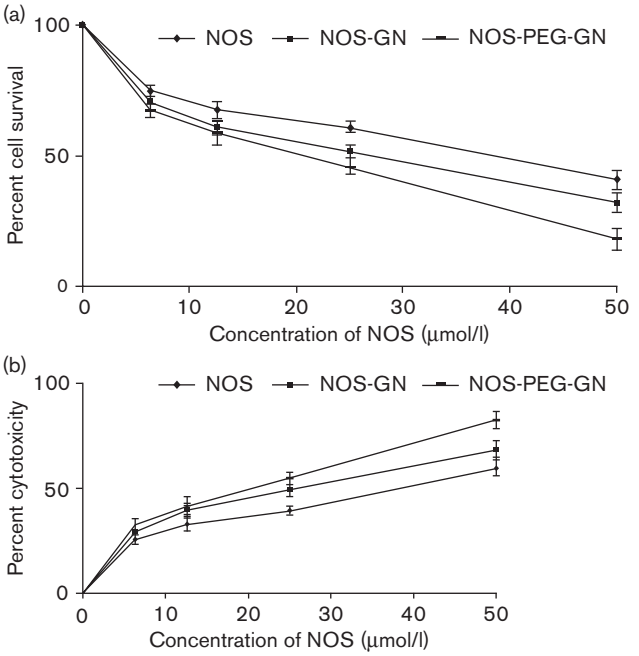

(a) Percentage cell viability of human breast cancer cell line (MCF-7) cells incubated with serial dilutions of noscapine (NOS), noscapine-loaded gelatin nanoparticles (NOS-GN) (GN1), and noscapine-loaded poly(ethylene glycol)-grafted gelatin nanoparticles (NOS-PEG-GN) (GN8). (b) Cell cytotoxicity of MCF-7 cells incubated with serial dilutions of NOS, NOS-GN (GN1), and NOS-PEG-GN (GN8). The IC_{50} value of NOS-PEG-GN was equivalent to 20.8 μmol/l, which was significantly ($P < 0.05$) lower than IC_{50} value of NOS-GN (26.3 μmol/l) and NOS (40.5 μmol/l). Values are shown as mean ± standard deviation for $n \geq 4$.

approximately 1.46-fold increase in the AUC_{last} for the PEG-modified formulation over the GN formulation and 13.40-fold increase over the NOS formulation. This, coupled with the observation that the PEG-modified formulation has a greater MRT in the plasma (2.97 h compared with GN with 2.45 h and NOS with 1.20 h), which is a confirmation of the stealth nature of NOS-PEG-GN that allow it to circulate for longer time in the plasma by avoiding RES uptake.

Cell cytotoxicity

The cytotoxicity profiles of NOS, NOS-GN (GN1), and NOS-PEG-GN (GN8) were examined using MCF-7 cell line by the MTT assay and their effect on cell survival and cell cytotoxicity was studied. For survival studies, cells were incubated with serial dilutions of free NOS and encapsulated NOS continuously and then washed to remove the drug and cell survival was determined after the addition of 6.25–50 μmol/l equivalent of NOS, respectively (Fig. 7a and b). Cytotoxicity analysis on MCF-7 cell line indicated that the IC_{50} value of NOS-PEG-GN (GN8) was equivalent to 20.8 μmol/l, which was significantly ($P < 0.05$) lower than the IC_{50} value of NOS-GN (GN1) (26.3 μmol/l) and NOS (40.5 μmol/l). The higher cytotoxicity and low IC_{50} value of NOS-PEG-GN (GN8) might be attributed to greater endocytosis of NOS-PEG-GN in breast cancer cells compared with NOS-GN and NOS [18].

Our systematic and methodological investigation of the synthesis parameters shows that it is possible to construct NOS-GN and NOS-PEG-GN with a narrow size distribution. Pharmacokinetic profiles of NOS, NOS-GN, and NOS-PEG-GN exhibited that NOS-PEG-GN has a greater half-life in comparison with NOS-GN and NOS due to stearic repulsion effect of PEG brush on nanoparticles. It is also encouraging to observe from the cytotoxicity profiles of NOS-GN and NOS-PEG-GN that these biodegradable polymers can deliver the anticancer drug to a greater extent in tumor cells in comparison with the parent molecule. Furthermore, these studies warrant further in-depth in-vitro and in-vivo studies for the delivery of NOS to cancer cells. Thus, we have presented here a viable formulation of NOS for systemic delivery to tumor cells.

Acknowledgements

The authors thank the Director, Sophisticated Analytical Instrumentation Facility, All India Institute of Medical Sciences, New Delhi, India for providing the facility of Transmission Electron Microscopy and Dr Sukesh Chand Sharma, Reader, Department of Biochemistry, Punjab University, Chandigarh, India for providing the gift sample of TNBS.

References

1 Landen JW, Lang R, McMohan SJ, Rusan NM, Yvon AM, Adams AW, *et al.* Noscapine alters microtubule dynamics in living cells and inhibits the progression of melanoma. *Clin Cancer Res* 2002; **62**:4109–4114.
2 Zhou J, Gupta K, Aggarwal S, Aneja R, Chandra R, Panda D, *et al.* Brominated derivatives of noscapine are potent microtubule-interfering agents that perturb mitosis and inhibit cell proliferation. *Mol Pharmacol* 2003; **63**:799–807.
3 Aneja R, Vangapandu SN, Lopus M, Chandra R, Panda D, *et al.* Development of a novel nitro-derivative of noscapine for the potential

Copyright © Lippincott Williams & Wilkins. Unauthorized reproduction of this article is prohibited.

treatment of drug resistant ovarian cancer and T-cell lymphoma. *Mol Pharmacol* 2006a; **69**:1801–1809.
4 Aneja R, Zhou J, Zhou B, Chandra R, Joshi HC. Treatment of hormone-refractory breast cancer: apoptosis and regression of human tumors implanted in mice. *Mol Cancer Ther* 2006b; **5**:2366–2377.
5 Olsson B, Bolme P, Dahlstrom B, Marcus C. Excretion of noscapine in human breast milk. *Eur J Clin Pharmacol* 1986; **30**:213–215.
6 Madan J, Dhiman N, Parmar VK, Sardana S, Bharatam PV, Aneja R, *et al.* Inclusion complexes of noscapine in β-cyclodextrin offer better solubility and improved pharmacokinetics. *Cancer Chemother Pharmacol* 2010; **65**:537–548.
7 Aneja R, Dhiman N, Idnani J, Awasthi A, Arora SK, Chandra R, *et al.* Preclinical pharmacokinetics and bioavailability of noscapine, a tubulin-binding anticancer agent. *Cancer Chemother Pharmacol* 2007; **60**:831–839.
8 Landen JW, Hau V, Wang M, Davis T, Ciliax B, Wainer BH, *et al.* Noscapine crosses the blood-brain barrier and inhibits glioblastoma growth. *Clin Cancer Res* 2004; **10**:5187–5201.
9 Vyas SP, Khar RK. *Controlled drug delivery: concepts and advances*. 1st ed. New Delhi: Vallabh Prakashan; 2001.
10 Gerweck LE, Seetharaman K. Cellular pH gradient in tumor Versus normal tissue: potential exploitation for the treatment of cancer. *Cancer Res* 1996; **56**:1194–1198.
11 Kreuter J. Evaluation of nanoparticles as drug delivery systems II: comparison of the body distribution of nanoparticles with the body distribution of microspheres (diameter/1 min), liposomes and emulsions. *Pharm Acta Helv* 1983; **58**:217–226.
12 Chasin M, Langer R. *Biodegradable polymers as drug delivery systems*. New York: Marcel Dekkaer; 1990.
13 Nakaoka R, Tabata Y, Ikada Y. Potentiality of gelatin microsphere as immunological adjuvant. *Vaccine* 1995; **13**:653–661.
14 Verma AK, Sachin K, Saxena A, Bohidar HB. Release kinetics from biopolymeric nanoparticles encapsulating protein synthesis inhibitor-cycloheximide, for possible therapeutic applications. *Curr Pharm Biotechnol* 2005; **6**:121–130.
15 Lee GY, Park K, Nam JH, Kim SY, Byun Y. Anti-tumor and anti-metastatic effects of gelatin–doxorubicin and PEGylated gelatin-doxorubicin nanoparticles in SCC7 bearing mice. *J Drug Target* 2006; **14**:707–716.
16 Lu Z, Yeh TK, Tsai M, Au JLS, Wientjes MG. Paclitaxel loaded gelatin nanoparticles for intravesical bladder cancer therapy. *Clin Cancer Res* 2004; **10**:7677–7684.
17 Cascone MG, Lazzeri L, Carmignani C, Zhu Z. Gelatin nanoparticles produced by a simple W/O emulsion as delivery system for methotrextate. *J Mater Sci Mater Med* 2002; **13**:523–526.
18 Kaul G, Amiji M. Long-circulating poly (ethylene glycol)-modified gelatin nanoparticles for intracellular delivery. *Pharm Res* 2002; **19**:1061–1067.
19 Kaul G, Amiji M. Biodistribution and targeting potential of poly(ethylene glycol)-modified gelatin nanoparticles in subcutaneous murine tumor model. *J Drug Target* 2004; **12**:585–591.
20 Maeda H, Noguchi Y, Sato K, Akaike T. Enhanced vascular permeability in solid tumor is mediated by nitric oxide and inhibited by both new nitric oxide scavenger and nitric oxide synthase inhibitor. *J Cancer Res* 1994; **85**: 331–334.
21 Sethi PD. *Analysis of drug in pharmaceutical formulations*. 1st ed. New Delhi: New Age Publishing Company; 1985.
22 Fields R. The measurement of amino groups in proteins and peptides. *Biochem J* 1971; **124**:581–590.
23 Azami S, Huang Y, Chen H, McQuarie S, Abrams D, Roa W, *et al.* Optimization of a two-step desolvation method for preparing gelatin nanoparticles and cell uptake studies in 143B osteosarcoma cancer cells. *J Pharm Pharm Sci* 2006; **9**:124–132.
24 Sherwood MA. Data analysis in X-ray photoelectron spectroscopy. In: Briggs D, Seah MP, editors. *Practical surface analysis*. 2nd ed. New York: John Wiley and Sons; 1990. pp. 555–586.
25 Gupta PK, Hung CT, Perrier DG. Quantitation of the release of doxorubicin from colloidal dosage forms using dynamic dialysis. *J Pharm Sci* 1987; **76**:141–145.
26 Illum L, Davis SS. The targeting of drugs parenterally by use of microspheres. *J Parenter Sci Technol* 1982; **36**:242–248.
27 Klimpel D, Cohon MS. pH of intravenous solutions. *New Engl J Med* 1969; **280**:900–901.
28 Desai MP, Labhasettwar V, Walter E, Levy RJ, Amidon GL. The mechanism of uptake of biodegradable microparticles in caco-2 cells is size dependent. *Pharm Res* 1997; **14**:1568–1573.
29 Zauner W, Farrows NA, Haines AM. In-vitro uptake of polystyrene microspheres: effect of particle, cell line and cell density. *J Control Rel* 2001; **71**:39–51.
30 Vandervoort J, Ludwig A. Preparation and evaluation of drug loaded gelatin nanoparticles for topical ophthalmic use. *Eur J Pharm Biopharm* 2004; **57**:251–261.
31 Saxena A, Sachin K, Bohidar HB, Verma AK. Effect of molecular weight heterogeneity on drug encapsulation efficiency of gelatin nanoparticles. *Colloids Surf B* 2005; **45**:42–48.
32 Mohanty B, Bohidar HB. Microscopic structure of gelatin coacervates. *Int J Biol Macromol* 2005; **36**:39–46.
33 Brahamnkar DM, Jaiswal SB. *Biopharmaceutics and pharmacokinetics-A Treatise*. 1st ed. New Delhi: Vallabh Prakashan; 1995.
34 Winter CA, Flataker L. Toxicities study on noscapine. *Toxicol Appl Pharmacol* 1961; **3**:96–106.

Copyright © Lippincott Williams & Wilkins. Unauthorized reproduction of this article is prohibited.